Quaternary Geochronology 74 (2023) 101422

Contents lists available at ScienceDirect

Quaternary Geochronology

journal homepage: www.elsevier.com/locate/quageo

Quartz OSL sensitivity from dating data for provenance analysis of pleistocene and holocene fluvial sediments from lowland Amazonia

Priscila E. Souza [a,*,1], Fabiano N. Pupim [b,c], Carlos E.M. Mazoca [c], Ian del Río [c], Thays D. Mineli [c], Fernanda C.G. Rodrigues [c], Naomi Porat [d], Gelvam A. Hartmann [a], André O. Sawakuchi [c]

[a] Instituto de Geociências, Universidade Estadual de Campinas, Campinas, SP, Brazil
[b] Departamento de Ciências Ambientais, Universidade Federal de São Paulo, Diadema, SP, Brazil
[c] Instituto de Geociências, Universidade de São Paulo, São Paulo, SP, Brazil
[d] Geological Survey of Israel, Jerusalem, Israel

ARTICLE INFO

Keywords:
Quartz luminescence sensitivity
OSL signal Deconvolution
Içá formation
Solimões river
Andean sediments
Amazon craton sediments

ABSTRACT

The properties of the quartz luminescence signal have been shown to be a useful tool for sediment provenance analysis. These provenance studies are based on the sensitivity of the fast optically stimulated luminescence (OSL) component, which is also used for sediment dating. Besides the widespread occurrence of quartz in terrigenous sediments, OSL sensitivity can be acquired using relatively fast and low-cost measurements compared to sediment provenance analysis methods based on accessory minerals or isotopes. Additionally, laboratories worldwide already have an extensive database of recorded quartz OSL signals primarily measured for dating studies, and these data could potentially be repurposed for provenance analysis of Quaternary sedimentary systems through OSL sensitivity calculation. Here, we investigate the use of OSL quartz signals measured in sediment dating surveys for OSL sensitivity calculation and evaluation of changes in sediment sources. The OSL sensitivity was calculated and expressed as $\%BOSL_F$, which corresponds to the percentage of the fast OSL component signal (blue stimulation) to the total OSL curve; such approach is advantageous as it does not require any normalisation of the measured signal intensity to dose or aliquot size (weight). Three sets of samples from Amazonian fluvial sediments are investigated: two sets of Holocene floodplain sediments representing different sediment sources to the Amazonian fluvial system, i.e. the Amazon craton and the Andes Mountain belt, and a set of samples from the Içá Formation, a paleo-fluvial system active during the Pleistocene whose provenance is not fully known. Results show that the quartz OSL signal derived from the first test doses (T_n) applied in dating protocols had the best performance for $\%BOSL_F$ calculation when compared to results from a measurement protocol designed specifically for sediment provenance analysis. There is significant correlation ($R^2 = 88$) between sensitivities derived from T_n and a specific OSL provenance analysis protocol. The proposed approach indicates to be appropriate for sediment provenance analysis since it is able to discriminate signal differences among samples from known sources: Brazilian cratonic quartz yield high sensitivity values (mean $\%BOSL_F > 70$), in contrast to the relatively lower values from Andean quartz (mean $\%BOSL_F < 50$). In general, quartz OSL sensitivities from the Içá Formation samples fall into the same range of modern sediments transported by the Içá and Japurá rivers draining the Andean Eastern Cordillera of Colombia and Ecuador. We also observe a decrease in quartz OSL sensitivity during the Holocene, notably after 4 ka, with younger deposits showing lower sensitivity. Sediment provenance variations are discussed in terms of watershed rearrangement and/or precipitation-driven changes during the Late Pleistocene and Holocene across Amazonia.

* Corresponding author. ,
E-mail address: pri.emerich97@gmail.com (P.E. Souza).
[1] Present address: Departamento de Ciências Ambientais, Universidade Federal de São Paulo, Diadema, SP, Brazil.

https://doi.org/10.1016/j.quageo.2023.101422
Received 18 August 2022; Received in revised form 18 January 2023; Accepted 19 January 2023
Available online 26 January 2023

1. Introduction

Characterizing the provenance of sediments is key for understanding changes in fluvial systems over time and space. In tropical settings such as Amazonia, continental-scale fluvial systems build and erode lowland terrains supporting diverse habitats for the biota (e.g. Sawakuchi et al., 2022). Variations in the sediment supply of the Amazonian fluvial system rely on marked changes in rainfall (Cheng et al., 2013; Häggi et al., 2017) and are of special interest to understand the distribution of upland and seasonally flooded terrains (e.g. Pupim et al., 2019) supporting specific habitats and their specialised biota (e.g. Ribas et al., 2012; Thom et al., 2020). The Içá Formation in central and western lowland Amazonia (Maia et al., 1977; Rossetti et al., 2015) records Pleistocene fluvial systems, whose floodplains were abandoned and converted into uplands (Pupim et al., 2019). Thus, constraining the provenance of the Içá Formation sediments would allow the identification of the sediment routing of the main fluvial systems responsible for this extensive sedimentary cover in the Amazon region.

Quartz grains are resistant and abundant minerals on Earth's surface. They have been extensively used for optically stimulated luminescence (OSL) dating of Quaternary sediments from a large range of depositional environments (e.g. Wintle, 2008; Wintle and Adamiec, 2017). Recently, it has been demonstrated that the luminescence properties of the quartz can also be a useful tool for sediment provenance analysis (Capaldi et al., 2022; Gray et al., 2019; Haddadchi et al., 2016; Sawakuchi et al., 2018, 2020; Tsukamoto et al., 2011). These provenance studies are based on the OSL sensitivity (i.e. the light emitted per unit mass per radiation dose) of the first second of the luminescence signal of the quartz. According to Pietsch et al. (2008), the quartz OSL sensitivity is related to the sediment transport history, as result of natural cycles of sediment transport (light exposure) and deposition (burial irradiation). Recently, Capaldi et al. (2022) have investigated the controlling factors on quartz OSL sensitivity (i.e. sediment history versus sediment source) for modern fluvial deposits, one of which relates to our study area, an Andean river and its tributaries. They have shown that quartz OSL sensitivity is an intrinsic property of the source rock for the modern Andean sediments (Capaldi et al., 2022). Similarly and previously, Sawakuchi et al. (2018) have shown that the OSL sensitivity of quartz grains under transport in Amazonian modern rivers reflects provenance as it discriminates sediments sourced by cratonic and orogenic areas. However, this approach was not extensively applied to ancient fluvial deposits so far.

The quartz OSL sensitivity applied in sediment provenance analysis has been routinely measured using the protocol proposed by Sawakuchi et al. (2018) (e.g. del Río et al., 2021; Mendes et al., 2019). Notably, a huge untapped database exists if Quaternary sediments studied worldwide and representing an extensive archive of quartz OSL signals measured for dating purposes could potentially be used for provenance analysis. However, how exactly could these data be repurposed from dating to sediment provenance analysis? This approach would also permit to obtain OSL sensitivity data already associated with sediment deposition ages, allowing to constrain changes in provenance through time.

Here, we test the use of data obtained in conventional OSL dating for sensitivity analysis aiming at provenance assessment of the Içá Formation and floodplains sediments of the Solimões River (Fig. 1),

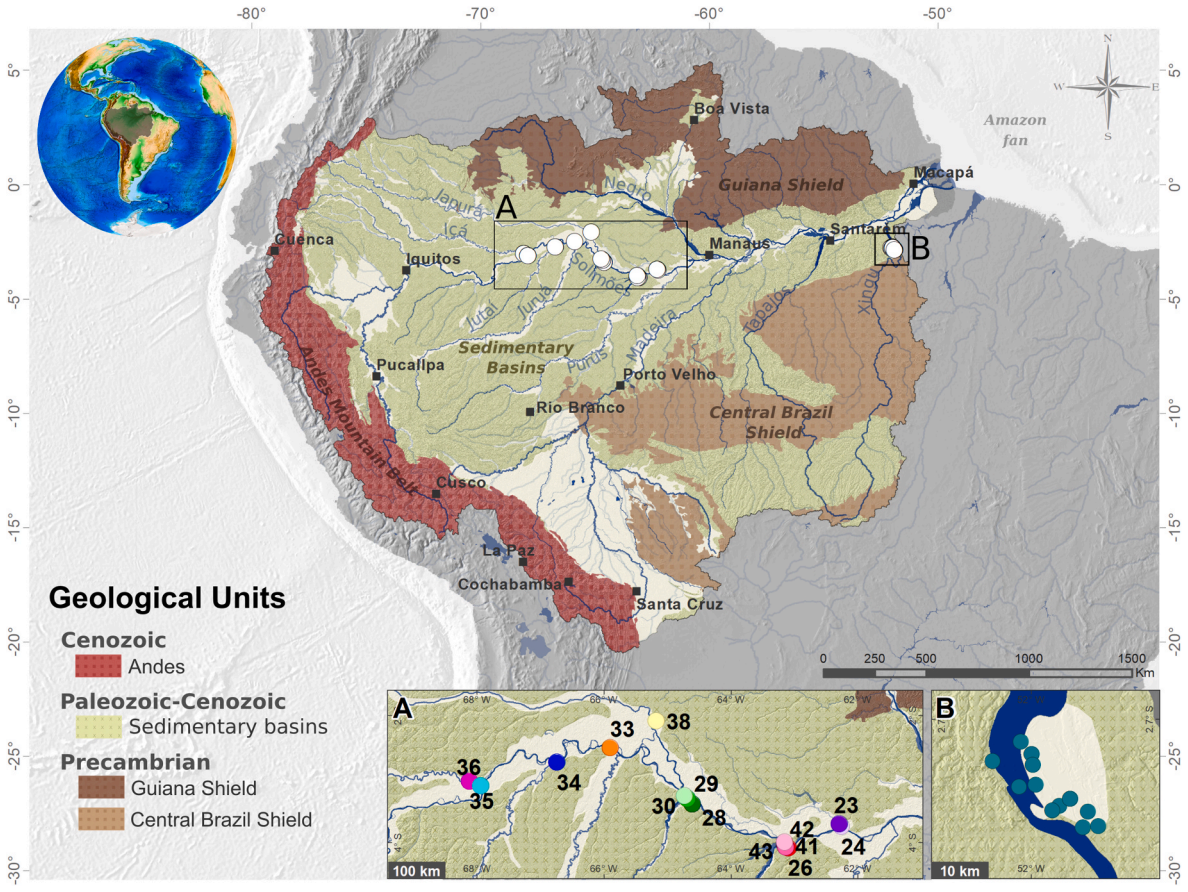

Fig. 1. Amazonian basin geological map (adapted from Schobbenhaus and Bellizzia, 2001) showing its mains river systems and sampling sites (white filled symbols). Geological units are represented in terms of their ages. Inset A shows in detail the location of cratonic samples endmembers from Xingu River floodplains. Inset B shows the location and identifies each sampling site along the Solimões River, which include both the Içá Formation (squares) and Andean samples endmembers (circles).

respectively recording Late Pleistocene and Holocene fluvial systems in western and central Amazonia. We validate our approach using modern sediment samples from Amazonian rivers in Brazil. Ultimately, we demonstrate a new and simple approach that provides relevant supplementary information about the provenance of sedimentary deposits that have already been dated, and benefits from the fact that neither additional sampling nor measurements are required, only data reanalysis.

2. Study setting

The Amazon River is the trunk river of an extensive system that drains terrains of different geological provinces, from the Cenozoic Andean orogenic belt, through the Amazon craton, represented by the Precambrian rocks of the Guiana and Brazilian shields and their Palaeozoic to Cenozoic sedimentary-igneous cover, including the Cenozoic fluvial deposits of the lowlands (Fig. 1). The headwaters of the Amazon River are located in the southern Peruvian Andes and its downstream segment in the Brazilian territory is the Solimões River, until the confluence with the Negro River, where the name changes to Amazon River (Fig. 1). The geological provinces drained by the Amazon River and its tributaries have diverse rock assemblages. The Andes comprises Mesozoic and Cenozoic metasedimentary and volcanic rocks, which supplied alluvial sediments accumulated in the Andean foreland basins (Jaillard et al., 2000). The Central Brazil and Guyana Shields host a complex array of medium to high grade metamorphic rocks (mainly schists, quartzites gneisses, and migmatites) and granitic rocks (Tassinari et al., 2000). These rocks are the basement of a sedimentary cover accumulated in cratonic basins during the Paleozoic and Mesozoic (Milani and Zalán, 1999). In these cratonic basins, stratigraphic units include terrigenous sedimentary rocks mainly represented by sandstones, siltites and shales, with local occurrence of evaporites and carbonates. Triassic basaltic sils associated with the Central Atlantic Magmatic Province occur within the Paleozoic sedimentary rocks (Heimdal et al., 2019).

Throughout its ~6500 km long course, the Amazon River connects with several tributaries, which are large rivers themselves. The Madeira River and tributaries on the Solimões left margin, such as the Içá and the Japurá rivers, have their headwaters in the Andes. The Juruá and Purus rivers are tributaries on the right margin of the Solimões River, and their headwaters are in the Neogene sediments of the Fitzcarrald Arch, an uplifted terrain of the Andean foreland zone (Espurt et al., 2009). Rivers with Andean headwaters are named as whitewater rivers (Sioli, 1984), which are responsible for most of the sediment load transported in the system (Filizola and Guyot, 2009; Milliman and Syvitski, 1992; Moquet et al., 2016) and their nutrient-rich fine sediments accumulate in large floodplains. In the central portion of the basin, the Solimões River meets the blackwater Negro River, the major river draining the Guiana shield. The clearwater Tapajós and Xingu rivers (Sioli, 1984) reach the Amazon River in the eastern portion of the basin and represent the main tributaries exclusively draining the Brazilian shield.

The area covered by Quaternary sediments in the lowland western and central portions of the Amazon River basin (Fig. 1) encompasses deposits of the Içá Formation and current fluvial plain. Içá Formation deposits occur as sand-dominated layers that were deposited during the Pleistocene and constituted the non-flooded *terra firme* interfluves, which are extensively distributed in the area as upland terraces (Pupim et al., 2019; Rossetti et al., 2015). Bordering these higher terrains, the floodplains of the Amazonian rivers are arranged as *várzeas* (whitewater rivers) or *igapós* (blackwater or clearwater rivers), and these silt and clay-dominant Holocene sequences are subject to seasonal flooding throughout the year. OSL ages from quartz grains were previously obtained for samples from the Içá Formation and the adjacent Holocene floodplain in sites of western and central Amazonia by Pupim et al. (2019) and for samples from Holocene fluvial bars on Negro, Tapajós and Xingu rivers by Sawakuchi et al. (2022).

Given its geographical location, near the Equator, the ocean moisture reaching Amazonia is related with the Intertropical Convergence Zone (ITZC) (Schneider et al., 2014), whose latitudinal position depends on the Atlantic ocean temperature gradient between South and North hemispheres. The precipitation over the Amazon River basin is driven by the South American Monsoon system (SAMS) (Zhou and Lau, 1998), which is active during austral summer. The SAMS precipitation experienced millennial variations over western and eastern Amazonia during the Holocene and late Pleistocene (Cheng et al., 2013; Wang et al., 2017), with marked influence on the fluvial sediment supply (Sawakuchi et al., 2022).

3. Methods

3.1. Data selection

The data used for OSL sensitivity calculation were already available in the database of the Luminescence and Gamma Spectrometry Laboratory (LEGaL) at the Institute of Geosciences of the University of São Paulo (USP). LEGaL research team has been studying sediments from the Amazonian basin since 2011, directing great effort into dating these sediments using quartz luminescence signals. Thus, the laboratory has an extensive database with recorded OSL signals that can potentially be repurposed for sediment provenance analysis.

We investigated two sets of samples from Holocene floodplain deposits with known sediment sources related to Andean and Brazilian cratonic rivers, and a third set of samples with unknown provenance from Late Pleistocene terraces bounding the Solimões River. The two Holocene sets are composed of samples from fluvial bars and floodplains of the Xingu and Solimões rivers (Fig. 1), with OSL ages presented in Sawakuchi et al. (2022). The Holocene deposits correspond to seasonally flooded plains, with sediment accumulation related to the active fluvial channels. Therefore, we regard them respectively as cratonic (Xingu) and Andean (Solimões) endmembers based on previous OSL sensitivity measurements on modern sands (Sawakuchi et al., 2018). The Pleistocene set is composed of samples from the Içá Formation, a palaeo-fluvial system in western and central lowland Amazonia (Pupim et al., 2019). In total, the data from quartz OSL dating of 14 samples representing the Içá Formation have been analysed; these data have been retrieved from measurements carried out by Pupim et al. (2019) (Fig. 1B). The cratonic endmember set is composed of 15 dated samples from the Tabuleiro do Embaubal archipelago representing stabilised sediment bars of the Xingu River (Fig. 1A) (Sawakuchi et al., 2022). The Andean endmember set is represented by data from four samples dated by Pupim et al. (2019) and eight samples from Sawakuchi et al. (2022) (Fig. 1B). A few sites are represented by more than one sample, collected in vertical sediment profiles and thus of different age. The criteria used for samples selection were: (i) samples measured in the same luminescence reader; (ii) test dose used in the Single Aliquot Regenerative dose (SAR) protocol was >0.5 Gy. See samples details in Table S1.

3.2. Sample preparation and measurements

The studied samples have been collected, prepared, and processed following standard procedures for quartz OSL dating purposes: wet sieving to isolate a specific sand grain size interval, treatments with 10% H_2O_2 and 10% HCl to eliminate organic matter and carbonate minerals, respectively, density separation using lithium metatungstate solutions at densities of 2.75 and 2.62 g/cm^3 to isolate light from heavy minerals and quartz from feldspar, treatment with 38% HF to remove the alpha irradiated layer of quartz grains and any remaining feldspar, and a final wet sieving to eliminate grains finer than the target grain size interval. For further details about the samples' preparation see Pupim et al. (2019) and Sawakuchi et al. (2022). Quartz OSL signals derive from medium pure quartz aliquots (100–300 grains) composed of grains in the sand fraction (63–125, 125–180, or 180–250 μm; see Table S1)

which were dated using a SAR protocol (Murray and Wintle, 2000) and/or measured through a OSL sensitivity protocol for provenance analysis (Table 1). The number of aliquots per sample used for OSL sensitivity calculation varied between 11 and 24 (dating data) and between five and six (data from OSL sensitivity protocol).

In all cases, luminescence signals were measured using a Risø TL/OSL DA-20 reader equipped with a $^{90}Sr/^{90}Y$ beta source, delivering a dose rate of ~0.1 Gy s^{-1}. The quartz aliquots were stimulated for 40s with blue LEDs (470 ± 20 nm) at 90% maximum power density (~40 mW cm^2) and the emitted light was detected in the ultraviolet band through a Hoya U-340 filter. Additional information used in the original dating sequence, such as applied thermal treatment and test dose size, are summarised in Table S1.

3.3. OSL sensitivity calculation and signal deconvolution

The quartz OSL sensitivity can be measured in absolute or relative terms. In the first case, it is necessary to know both the given dose and the aliquot mass, and the sensitivity is expressed as counts per mass per Gy (cts mg Gy^{-1}). In the second case, the sensitivity is expressed as a percentage of the total light emitted during the optical stimulation time measured OSL curve and, therefore, the aliquot mass is not relevant. Since we are working with old data, obtained from aliquots of unknown weight, the sensitivity was calculated in relative terms here.

The sensitivity, hereafter regarded as $\%BOSL_F$, was calculated by dividing the integral of the first second of light emission from the blue OSL ($BOSL_{[1s]}$) curve presumed to be dominated by the fast OSL component (Jain et al., 2003), by the integral of the total blue OSL curve ($BOSL_{[total]}$), both subtracting the respective normalised background. Here, we assumed a late background: the mean of the last 10s of the OSL curve times the number of channels of the respective assessed "signal" (i.e. $BOSL_{[1s]}$ or $BOSL_{[total]}$). The $\%BOSL_F$ was calculated only for light intensity (1s) at least three standard deviations above the background; those that fell to comply with this criterion were classified as "dim" and were not included in the calculation of the sample mean $\%BOSL_F$. Recycling and recuperation criteria used for aliquot validation in dating were not applied. All calculations, including the filter used to reject dim samples, were quickly performed (less than 3 min per binx. file) using a routine we designed in RStudio with the Luminescence Package (Kreutzer et al., 2012). The routine we designed is available as a supplementary material.

Additionally, the OSL decay curve was deconvoluted to isolate the contributions from the different OSL components in relation to the total $BOSL_{[1s]}$. We assume an OSL curve composed of three components, a fast, medium, and slow component, despite previous studies propose the existence of higher number of fast (ultrafast), medium, and slow components (e.g. Bailey et al., 1997; Jain et al., 2003; 2008). Additionally, the proportion of OSL components is affected by their thermal stability (Jain et al., 2003). However, the dominance of the fast OSL component in the first second of blue OSL stimulation is sample dependent (Jain et al., 2003) and related to bleaching and irradiation cycles (Moska and Murray, 2006). Assuming a three OSL components view, we use here the relative proportions of fast, medium, and slow OSL components to complement the analysis of discrimination of quartz from Andean and cratonic sources. Despite a higher number of components could better describe the quartz OSL emission (e.g. Jain et al., 2003), the three components assumption supports the practical approach used to discriminate quartz grains by using the relative proportion of the fast OSL component in relation to other medium and slow components. Deconvolution was performed using the Fit_CWCurve function (Kreutzer, 2020) based on Equation (1) (Bøtter-Jensen et al., 2003) assuming three components (fast, medium, and slow):

$$I_{OSL(t)} = n_1 p_1 \exp_1^{-tp} + n_2 p_2 \exp_2^{-tp} + n_3 p_3 \exp_3^{-tp} \quad \text{(Equation 1)}$$

where I_{OSL} is the OSL intensity, $n_{1,2,3}$ is the initial concentration of trapped electrons (m^{-3}), $p_{1,2,3}$ is the rate of stimulation (s^{-1}), and t is the time of stimulation (s). The Fit_CWCurve function is a beta version and thus it has not been properly tested yet; its authors alert that the parameter used to be describe the goodness of the fit may not be the best parameter and, therefore, "the function does not ensure that the fitting procedure has reached a global minimum rather a local minimum" (Kreutzer, 2020). We used this function nevertheless, assuming it may not be the most appropriate, because here this analysis is complementary to the main data that we are focusing on for provenance fingerprinting (i.e. $\%BOSL_F$).

3.4. Validation of OSL sensitivity from dating measurements

Firstly, we calculated sensitivity ($\%BOSL_F$) based on signals from the SAR protocol (Table 1) – i.e. OSL signals derived from the natural (L_n), regenerative (L_x), and test doses (T_n and T_x). Such experiment gives the basis for deciding which signal from a dating sequence should be prioritised for OSL sensitivity calculation and, thus, used for sediment provenance analysis. This experiment was performed with OSL dating data of five samples from the Içá Formation: ALC-26 B, ALC-28 F, ALC-33C, ALC-34 A, and ALC-35 A.

Then, we validated our approach by comparing $\%BOSL_F$ values from the same samples but obtained from a sensitivity protocol or dating protocols. This experiment was performed for representative samples from the Içá Formation (n = 5, ALC samples) and from Xingu River (n = 3, EMB samples), in which five fresh aliquots of each sample containing about ~200 grains were measured using the sensitivity protocol (Table 1; Sawakuchi et al., 2018). The purified quartz grains of these samples had been stored in the LEGaL sample repository and were ready-to-use. The size of the given dose in the sensitivity and dating protocol measurements were the same, but sample specific: 0.56 Gy for EMB13-1 A, EMB13-09 B, and EMB13-09 A; 11 Gy for ALC-26 B, ALC-28 F, and ALC-35 A; 20 Gy for ALC-34 A; 34 Gy for ALC-33C. Finally, we compared the $\%BOSL_F$ of the Pleistocene Içá Formation samples to those of the endmember samples and deduced the sediment source for this formation.

Table 1
OSL dating and OSL sensitivity (provenance analysis) protocols used for the comparative test with representative samples. Test dose size was sample dependant, as specified in the text (section 3.4). Test results are shown in Fig. 3. The highlighted treatments (in bold) correspond to the quartz OSL signal used for sensitivity calculation.

Step	Dating Protocol	Sensitivity Protocol
1	Dose	Bleaching: Blue LEDs @ 125 °C for 100s
2	Preheat @ 200 °C for 10s	Dose
3	Blue OSL @ 125 °C for 40s (L_n)	Preheat @ 190 °C for 10s
4	Test dose	IR @ 60 °C for 300s
5	Preheat @ 160 °C for 0s	**Blue OSL @125 °C for 100s (L_x)**
6	**Blue OSL @125 °C for 40s (T_n)**	–
7	Back to step 1	–

4. Results

4.1. Comparison of OSL sensitivities from different SAR doses

Dating data of five Late Pleistocene samples from the Içá Formation (Pupim et al., 2019) were analysed to calculate $\%BOSL_F$ from signals derived from the natural (L_n), regenerated (L_x) and test doses (T_n and T_x) of 18–24 aliquots (per sample) over the SAR cycles (Fig. 2).

In all cases, the L_x signals have 10–20% higher $\%BOSL_F$ than the T_x signals. For instance, in the case of sample ALC-26 B, the mean $\%BOSL_F$ derived from L_x is ~58% while the T_x counterpart is ~40%. Comparisons among $\%BOSL_F$ values derived from different SAR cycle doses signals show that, on average, the $\%BOSL_F$ derived from L_n is 26% higher than that from L_1, and the $\%BOSL_F$ given by T_n is 14% smaller

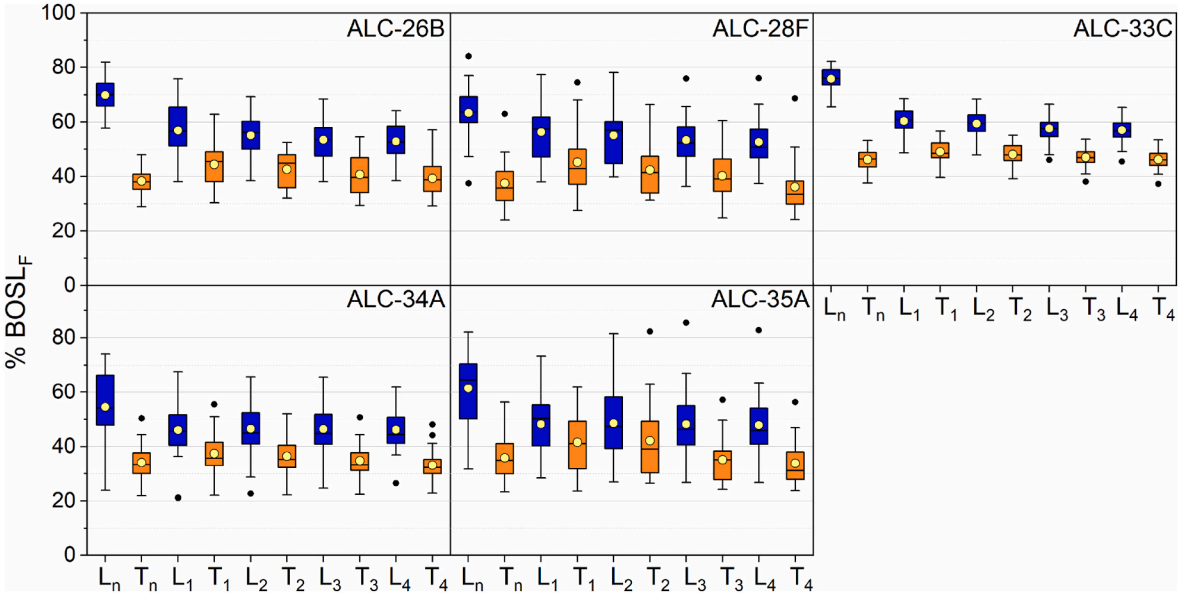

Fig. 2. Boxplots of quartz OSL sensitivities (%BOSL$_F$) calculated from natural (L_n), regenerated (L_x), and test (T_n and T_x) doses for five Içá Formation samples. Blue and orange boxes represent L_n or L_x and T_n or T_x data, respectively. Each pair of L and T data corresponds to a SAR cycle from the dating protocol; thus $L_1<L_2<L_3<L_4$ while $T_n = T_1 = T_2 = T_3 = T_4$. Yellow and black dots correspond to mean and outlier values, respectively.

than that by T_1 (Table 2). These differences, however, are significantly smaller (<3%) between regenerative-dose cycles and %BOSL$_F$ is nearly constant through the SAR regenerative cycles (Table 2).

We decided to continue our experiments using the quartz OSL signal derived from the first test dose (T_n), i.e. from the test dose administered after the natural OSL signal measurement. At this step, the aliquot has been subjected to the least number of treatments that could potentially change the natural OSL sensitivity. In fact, the type and number of thermal and optical treatments that the aliquot is subjected to until this point is the most similar to those applied in a sensitivity measurement protocol (Table 1).

4.2. Protocols comparison

Results of the comparison between %BOSL$_F$ values derived from signals of five samples measured with both the sensitivity analysis protocol (four to five aliquots per sample) and the OSL dating protocol (using T_n signal data, six aliquots per sample) are shown in Fig. 3. There

Table 2
Ratios between mean %BOSL$_F$ values derived from natural (L_n), regenerated (L_x) or test (T_n and T_x) doses of subsequent SAR cycles. Number of aliquots (n): 23 (ALC-26 B), 21 (ALC-28 F), 24 (ALC-33CC and ALC-34 A), and 18 (ALC35-A). The last column corresponds to the average of the ratios presented in each row.

Ratio	ALC-26 B	ALC-28 F	ALC-33C	ALC-34 A	ALC-35 A	Mean ± SE
L_1/L_n	0.81	0.92	0.80	0.85	0.83	0.84 ±0.020
L_2/L_1	0.98	0.95	0.98	1.01	0.99	0.98 ±0.010
L_3/L_2	0.97	0.97	0.97	1.00	0.98	0.97 ±0.006
L_4/L_3	0.98	0.98	0.99	0.99	0.99	0.98 ±0.002
T_1/T_n	1.16	1.22	1.06	1.10	1.14	1.14 ±0.030
T_2/T_1	0.95	0.92	0.98	0.97	1.02	0.97 ±0.020
T_3/T_2	0.96	0.95	0.98	0.95	0.83	0.93 ±0.020
T_4/T_3	0.98	0.92	0.98	0.95	0.93	0.95 ±0.010

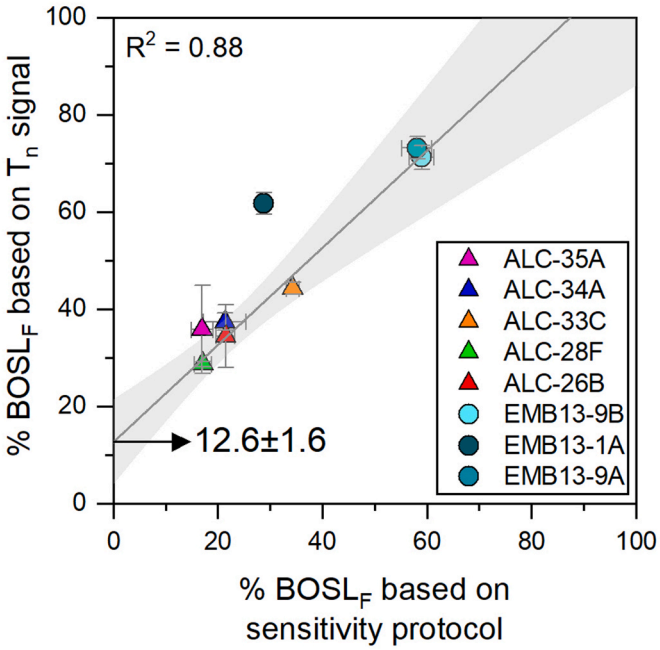

Fig. 3. Comparison between %BOSL$_F$ values derived from the sensitivity protocol measurements (regenerated signal) and dating data (T_n signal), both measured in the same reader. The linear fitting line through the points is forced to have a slope 1, weighted by the error bars.

are relatively few aliquots from the OSL dating data (different n than that given in Table S1) because this experiment was performed from scratch, employing both protocols to fresh aliquots (i.e. never measured), using the same reader (same sequence), with no possible drift of performance of any part of the measurement system (e.g. PMT, strength of diodes, which does weaken over time).

Mean %BOSL$_F$ values derived from both protocols show a significant correlation ($R^2 = 0.88$) and the data points adjust well to a linear fit with a 1:1 fixed slope. However, the data indicate a systematic positive offset in the y-axis of 12–30% (taking error bars into account); if we assume at

face value the intercept given in the y-axis by the linear fit with a slope of 1, the data indicate that mean $\%BOSL_F$ values derived from T_n data are ~12% higher than those from the sensitivity protocol (Fig. 3). Both protocols use regenerated signals, therefore such offset should not be related to the nature of the signal (i.e. natural versus laboratory irradiation); instead they may arise from differences in thermal treatments applied (Table 1), which are discussed later in the text.

4.3. Provenance analysis

Finally, the $\%BOSL_F$ of all samples from the Içá Formation, Holocene sediments from Xingu and Solimões rivers were calculated using the T_n signals. Endmembers from Xingu and Solimões rivers provided $\%BOSL_F$ mean values sufficiently different to distinguish between cratonic and Andean sources (Fig. 4). Additionally, our results are in accordance with what has been reported for riverbed sediments of the Xingu and Solimões rivers (Sawakuchi et al., 2018): Holocene Xingu quartz grains show higher $\%BOSL_F$, with values higher than 70% (dataset mean $\pm1\sigma$ = 79.0 ± 1.0%), characteristic of cratonic sources, while Holocene Solimões present lower quartz OSL sensitivity, typical of Andean quartz of less than 50% (dataset mean $\pm1\sigma$ = 40.3 ± 1.2%) (Fig. 4). Based on these results, we propose the following thresholds: $\%BOSL_F$ mean value < 50% is classified as "lower"; 50–70% is classified as "moderate"; and >70% is classified as "higher" OSL sensitivity. This classification is further applied to sediment provenance as Andean, mixed Andean-cratonic, or cratonic, respectively.

Mean $\%BOSL_F$ values of Içá Formation samples range from 31.9 ± 1.9 to 46.2 ± 0.8% (mean $\pm1\sigma$ = 35.6 ± 0.9%), which fall into the range classified as lower sensitivity quartz (Fig. 4), typical of an Andean source. We observe that one sample, ALC-33C (orange box in Fig. 4), stands out from the other Içá Formation dataset, presenting a relatively higher mean $\%BOSL_F$ (46.2 ± 0.8%). Although higher, this value is still in the same range as the Solimões Holocene representatives and, thus, based on the classification presented above, this sample is also considered to have lower $\%BOSL_F$ sensitivity.

Results from the OSL signal deconvolution from 18 representative samples, six from each dataset (Içá Formation, Andes, and Amazon craton), strengthen the differences and similarities among studied sediments (Fig. 5). The first second of light emission of quartz from Andean endmembers is composed, on average, of 43% of the fast, 27% of the medium, and 30% of the slow OSL components (central graphs in Fig. 5). Cratonic endmembers, on the other hand, are dominated by the fast OSL component (~70%) and show little contribution (~20%) of the slow OSL component (graphs on the right, Fig. 5). In general, the contribution of each OSL component is almost even (27–34%) in the Içá Formation samples (left column, Fig. 5).

5. Discussion

Data from OSL dating sequences have been successfully repurposed for use in sediment provenance analysis. Our approach suggests being valid, as it yields results in accordance with those reported using the established quartz OSL sensitivity method for provenance analysis in modern riverbed sediments (e.g. Sawakuchi et al., 2018) (Fig. 3). Moreover, it benefits from the fact that neither additional sampling nor luminescence measurements are required, allowing to derive sediment provenance information coupled with OSL ages. Such simple, fast, and low-cost analysis could well be performed using data from previous OSL dating surveys.

Apparently, the thermal, optical, and dosing treatments that the aliquots are subject to in each regenerative-dose cycle from a SAR protocol do not significantly change $\%BOSL_F$ of the samples employed in this study (Fig. 2) when signals of the same type (natural, regenerative or test doses) are compared to each other. Mean $\%BOSL_F$ values given by L_x signals from different SAR cycles are nearly constant, and the same is observed for $\%BOSL_F$ from T_x signals (Fig. 2 and Table 2). Main differences arise when we directly compare signals of natural dose *versus* regenerative dose or signals that have been subjected to different thermal treatments. The differences observed between $\%BOSL_F$ derived from natural and regenerative cycles (e.g. L_n *versus* L_1, and T_n *versus* T_1), which received the same thermal treatment, could be related to variations in rates of charge generation and trapping between natural and laboratory irradiation (e.g. Peng et al., 2022). Our results suggest that $\%BOSL_F$, i.e. the proportionality of the fast fraction to the total signal, is a conservative property and, thus, we could probably have worked with mean sensitivity values calculated from all test dose signals (T_n, T_1, T_2, etc.) and not only from T_n signals. However, the $\%BOSL_F$ stability might be a peculiarity of these studied samples, because cycles of irradiation and bleaching are expected to cause sensitivity changes, increasing the signal intensity (e.g. Moska and Murray, 2006; Murray and Wintle, 2000). The sensitivity changes throughout SAR cycles seem to be sample-dependent (Fig. 2, Table 2), but the laboratory OSL signal obtained under a reduced number of irradiation, thermal and/or optical stimulation treatments (and thus the least altered) is the signal derived from the first test dose (T_n). Therefore, in order to ensure that the proposed approach works universally, we recommend that, in all cases, the T_n signal should be used for OSL sensitivity calculation.

The differences in Fig. 3 indicate that we cannot use the same thresholds reported in the literature, based on the sensitivity protocol, for classifying the Andean or cratonic Amazonian fluvial sediments in terms of standard $\%BOSL_F$ values, because our approach overestimates the previously reported values. For instance, Sawakuchi et al. (2018) consider as "low sensitivity" those $\%BOSL_F$ values < 30%, but such threshold in our approach would be of approximately <40%, if the ~12% offset observed in the protocols' comparison experiment (Fig. 3) is accounted for. The cause for the offset we observe is probably related

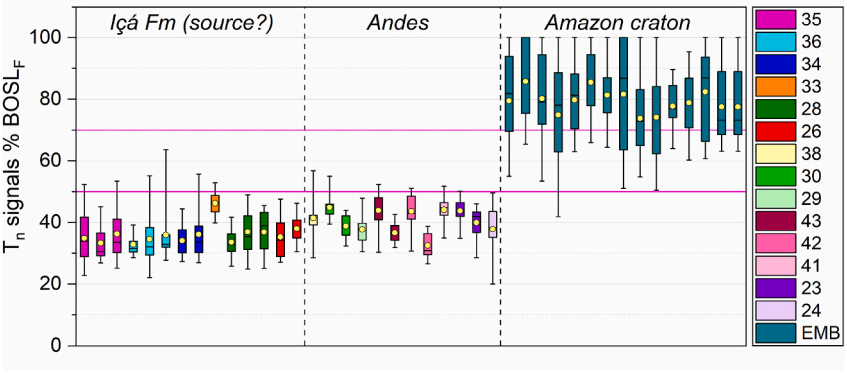

Fig. 4. Summary of the $\%BOSL_F$ results derived from T_n signals for all studied samples. Vertical dashed lines separate the three sets of samples: Içá Formation endmembers (to the left, whose source we are investigating), Andean Holocene endmembers (centre), and cratonic Holocene endmembers (right). Yellow filled circles indicate the mean values of each dataset. Horizontal magenta lines indicate the thresholds suggested in this study for classifying the sensitivity mean values as lower (<50%), moderate (50–70%), and higher (>70%). Except for Xingu samples (EMB), which are represented by one colour alone, boxplots colours represent samples collected at the same site, but at different depths and, thus, of different ages (Table S1). Numbers on the legend correspond to the numerical index used for ALC samples (i.e. from Içá Formation and Andean endmembers, ALC-35 for example), also used in Fig. 1B to indicate the sampling sites' location.

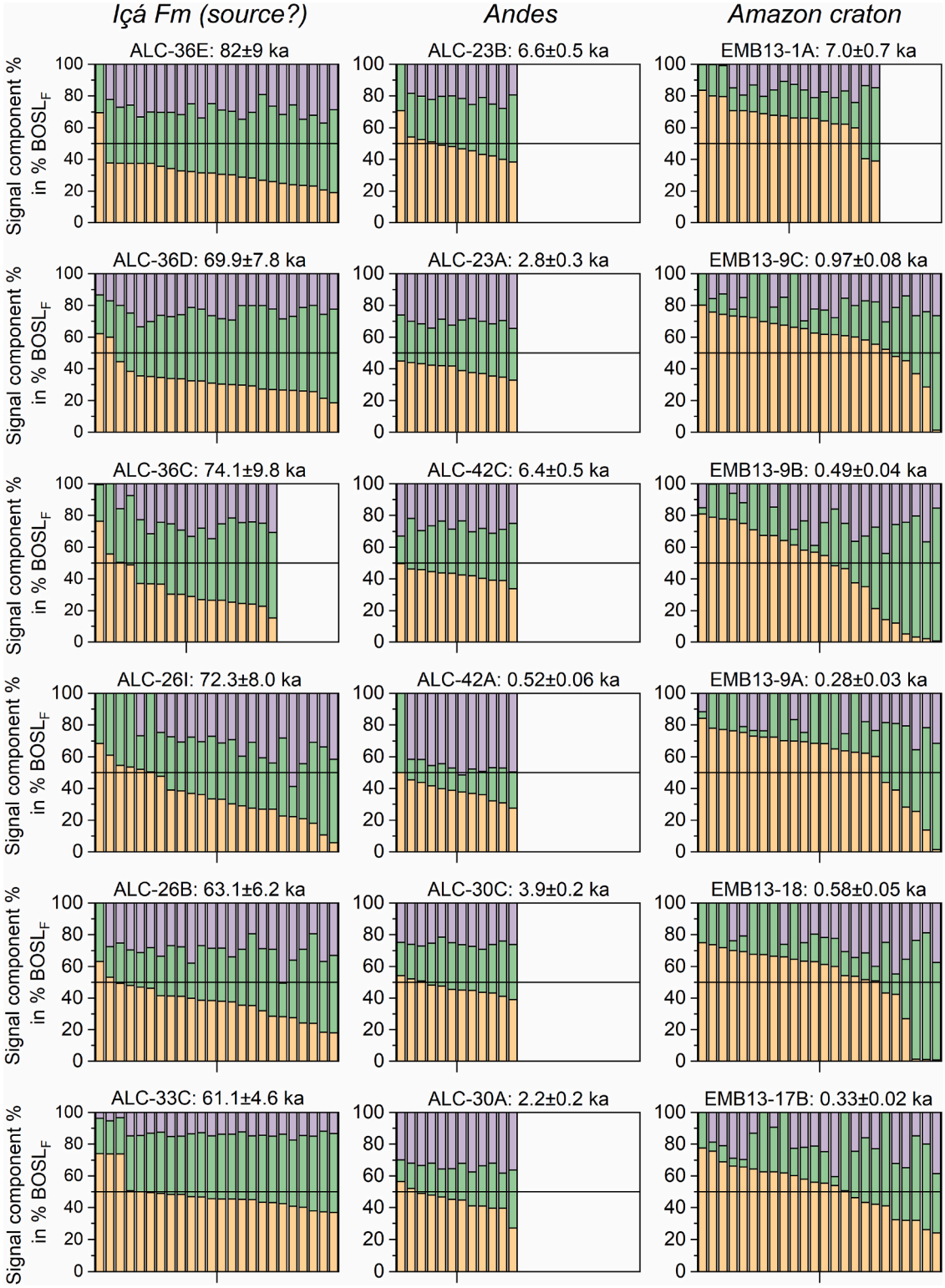

Fig. 5. Signal components contribution (%) in %BOSL$_F$ (first second of light emission) of representative samples from the Içá Formation (left column), and from the Andean (centre) and the cratonic (right) endmembers. Each composite vertical bar represents the OSL curve from an aliquot, and the colours identify the signal component: fast (orange), medium (green), and slow (purple). 12 to 24 OSL curves per sample were analysed; the tick on the x-axis marks the middle of the dataset. Data shown here were obtained from re-analysing OSL dating data from previous works, all measured in the same reader (Table S1).

to differences in the thermal treatment employed in each protocol. First, the T_n signal received two preheats whereas the sensitivity measurement only one (Murray and Wintle, 2000); second, and perhaps more importantly, the T_n signal preheat is, in fact, a cutheat at 160 °C (0s) while in the sensitivity protocol the preheating is at 190 °C for 10s (Table 1). This second observation evokes the findings by Sawakuchi et al. (2020). These authors have employed a range of preheat temperatures for quartz OSL sensitivity measurements and have observed that the sensitivity decreases as the preheat temperature increases, but sensitivity differences among samples are not affected by the preheat

temperatures. Here, all T_n signals used for quartz OSL sensitivity calculation were measured after the same (cutheat) temperature (Table S1), including those representing endmembers categories; therefore, the sensitivity differences among samples should be preserved and they should represent differences in sediment provenance. Differences between the OSL sensitivity protocol and the approach we propose here do not hinder the use of OSL dating data for sediment provenance analysis, although it shows that caution must be practised when comparing data from studies that used different measurements approaches, as well as when comparing sensitivity data from OSL signals obtained after different thermal treatments and/or obtained from different luminescence readers.

The sensitivity values obtained for the Late Pleistocene Içá Formation sands resemble those of the Andean endmembers, being characterised quartz grains with relatively lower mean $\%BOSL_F$ (<50%) and a significant contribution of the slow component (>25%) to the first second of light emission. In fact, most $\%BOSL_F$ values from the Içá Formation samples are even lower and with a more pronounced contribution from the slow component than the Andean endmembers represented by modern sediments transported by the Solimões River (except for sample ALC-33C, Figs. 4 and 5). Such findings might indicate that either previously defined Andean endmembers have some contribution from other tributaries that drained cratonic areas (or cratonic sediments stored in ancient terraces), or that their Andean quartz grains (those older than 2 ka, Fig. 6) have been somehow more sensitised. Additionally, Fig. 6 shows that the OSL sensitivities obtained for Late Pleistocene Içá Formation samples have reduced variation, in contrast to the Holocene floodplain sediments, which is more scattered. Such observation may indicate that the Içá Formation sediments had higher mixing or/and had a smaller watershed and more specific source over time (~110–50 ka), while the Holocene watershed integrates tributaries from diverse sources and sediment reworking from riverbank deposits. A trend toward more Andean sources is also observed in the floodplain sediments from around 8 ka to 0.52 ka (Fig. 6).

The fact that ALC-33C sample stands out from its group, being more similar to the early to mid-Holocene Solimões sediments, is puzzling. This sample presents a higher mean sensitivity than its Pleistocene counterparts (Fig. 6), its relative contribution from the different signal components is more homogeneous among aliquots (Fig. 5), and its $BOSL_F$ is dominated by the fast component (Fig. 5). ALC-33C sample was collected from a terrace near the confluence of the Solimões River and Juruá River (Fig. 1), a large southern tributary with sub-Andean sediment source, whose mid and low course varied considerably over the Pleistocene, once having its point of confluence with Solimões more to the west of its present position (Ruokolainen et al., 2019). Sawakuchi et al. (2018) have characterised the quartz OSL sensitivities of polymineral silt from the riverbed of the Juruá River and have found relatively higher sensitivity than the Solimões riverbed silt. In fact, the OSL sensitivity values calculated for Juruá samples are in the same range of those from the Negro River, which is considered to have mixed Andean and cratonic sediments (see Fig. 2A in Sawakuchi et al., 2018). We suggest that the relatively higher sensitivity and the homogeneity observed in ALC-33C sample indicate that the paleo-watershed recorded in the Late Pleistocene Içá Formation also included cratonic tributaries. In this sense, it is reasonable to expect to see the same provenance influence on other samples collected downstream of Juruá's mouth. The Pleistocene sediment samples ALC-28 and ALC-26 were collected in Tefé and Coari rivers, ~200 and 400 km to the east of Juruá's mouth, respectively (Fig. 1B), however their sensitivities do not resemble that observed for ALC-33C sample (Fig. 6). On the contrary, the sensitivities of ALC-28I, ALC-28H, ALC-28 F, ALC-26I, and ALC-26 B samples are in the same range (i.e. 30–40%, Fig. 6) as those of other Late Pleistocene samples collected upstream Juruá mouth and ALC-33C sample site (see sites location in Fig. 1B).

In summary, the studied Içá Formation in lowland Amazonia presents quartz OSL sensitivity values characteristic of Andes-derived sediments, as observed for modern sediments from Solimões, Içá, and Japurá rivers (Sawakuchi et al., 2018). We hypothesized that higher precipitation variability in western Amazonia (Cheng et al., 2013) allowed periods of increased erosion rates and favoured Andean sediment input to the Amazon lowlands during the deposition of the Içá Formation (110–45 ka).

The period between 45 and 8 ka is marked by channel incision and deposits that were not sampled in previous studies, hindering the interpretation of sediment sources during this time interval. From ~8 to 4 ka, the sensitivity values are in the same range as that observed for sample ALC-33C (i.e. >40%), but after ~4 ka there is a trend of OSL sensitivity decrease as the deposits get younger (Fig. 6). For instance, ALC-30C sample (age 3.94 ± 0.26 ka, Table S1) has a $\%BOLS_F$ of 45 ± 2.2%, while the sensitivity of ALC-30 A sample (age 2.19 ± 0.17 ka, Table S1) is 39.2 ± 1.5%. Based on the OSL sensitivity values from modern silt samples (Sawakuchi et al., 2018), the $\%BOLS_F$ values observed in the early to mid-Holocene samples suggest contribution from lowland sub-Andean or cratonic rivers (Juruá and Jutaí rivers). The observed OSL sensitivity change during the late Holocene corroborates the findings by Hoppner et al. (2018), who suggested that the main sediment source to the Amazon River system has changed during the late Holocene, becoming more dominated by Andean sediments directly transported from the headwaters of the Solimões and its main Andean tributaries.

We suggest that changes in the precipitation conditions in the western Amazonia, which have altered the erosion rates and Andean sediment supply to lowlands, may be the reason for this quartz OSL sensitivity decreasing throughout the Holocene, notably after 4 ka.

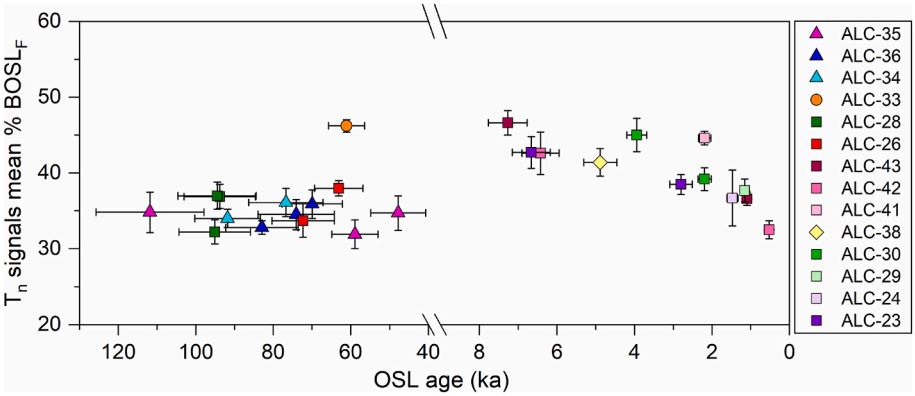

Fig. 6. Mean $\%BOSL_F$ (±SE) from T_n signals *versus* OSL ages. Ages are compiled from Pupim et al. (2019) (ALC-35, 36, 34, 33, 28, 26, 23, and 24) and Sawakuchi et al. (2022) (ALC-29, 30, 41, 42, and 43). Triangles and squares represent samples collected at sites upstream and downstream of the mouth of Juruá River, respectively. ALC-33C (orange circle) is a deposit near Juruá's mouth and ALC-38 (yellow diamond) is located at Japurá River, before it meets with Solimões River.

Paleoprecipitation data seems to support our interpretation. In general, in western Amazonia, the early and middle Holocene is characterised by drier conditions in relation to the Last Glacial Maximum (LGM, ~21 ka) and deglacial period, and it was only after ~4 ka that the western Amazonia has experienced a noticeable and relative (to the LGM) increased precipitation (Baker et al., 2001; Cheng et al., 2013; van Breukelen et al., 2008). In fact, Baker et al. (2001) report that maximum aridity and the lowest water level of Titicaca Lake, which would represent the climate conditions in the headwaters of the Solimões River, occurred between 8000 and 5500 cal yr B.P. The Holocene climate records for the western Amazonia based on $\delta^{18}O$ values of speleothems by van Breukelen et al. (2008) indicate relatively wetter and more stable conditions since 2 ka. Such scenario of increased precipitation since ~4 ka may have promoted a new phase of more pronounced erosion in catchment areas of western Amazonia, increasing the supply of Andean sediments to the Solimões River, which could then explain the observed $\%BOLS_F$ decrease trend over time (Fig. 6).

6. Conclusions

We proposed a new approach for investigating sediment provenance based on quartz OSL sensitivity derived from data originally measured for dating purposes. The method proved to be fast and reliable, having the great advantage of providing sediment provenance information associated with depositional ages, which allows for temporal positioning. The OSL sensitivity based on the fraction of the signal dominated by the fast OSL component (first second of light emission) to the total OSL, $\%BOSL_F$, has the great advantage over that based on signal intensity, previously used, because it does not require any normalisation to dose or weight (aliquot size), data which is not always available. Moreover, our approach suggests that the $\%BOSL_F$ might be a conservative parameter throughout SAR cycles. However, it would be interesting to verify such observation using more samples from different geological contexts worldwide.

The fluvial system active during deposition of the Içá Formation (110–50 ka) in the study area had a higher contribution of Andean rivers sediments, similar to the modern Içá and Japurá rivers. The contribution of lowland sub-Andean or mixed rivers increased from 8 to 4 ka and reduced again in the late Holocene. These variations in provenance could indicate shifts in river courses flowing over soft sedimentary substrates of Amazonian lowlands or changes in the relative sediment supply between Andean and lowland sources driven by precipitation variations.

Such findings, derived from OSL dating data reanalysis, are encouraging. OSL dating laboratories worldwide are shown the possibility of taking advantage of their extensive OSL dating archives, by repurposing OSL dating data into new data for quartz provenance analysis that is valuable for geological and landscape evolution studies. Apropos, we would encourage authors and/or OSL laboratories worldwide to provide the. bin (.binx) files on online repositories, allowing others to explore them beyond dating.

Declaration of competing interest

The authors declare that they have no known competing financial interests or personal relationships that could have appeared to influence the work reported in this paper.

Data availability

Data will be made available on request.

Acknowledgements

We are grateful for the commentaries and suggestions by Dr. Harrison Gray and by another anominous reviewer which helped improving this manuscript. This research had financial support from São Paulo Research Foundation (FAPESP) (grant #2018/23899–2; grant #2020/11047–1). The first author thanks Brazilian National Council for Scientific and Technological Development (CNPq) for funding her post-doctoral scholarship (#160670/2019–5), under which this study was most developed, and FAPESP for funding her current post-doctoral research that follows up the former (#2021/14022–2). CEMM thanks CNPq (#426654/2018–8) for funding field trips and laboratorial analysis. IdR was supported by FAPESP grant #2019/20588–9. AOS (#304727/2017–2), GAH (#312737/2020–3), FNP (#307262/2021–9) are research fellows of CNPq, Brazil. FCGR was supported by FAPESP (grant #2018/12472–8).

Appendix A. Supplementary data

Supplementary data to this article can be found online at https://doi.org/10.1016/j.quageo.2023.101422.

References

Bailey, R.M., Smith, R.M., Rhodes, E.J., 1997. Partial bleaching and the decay form characteristics of quartz OSL. Radiat. Meas. 27, 123–136. https://doi.org/10.1016/S1350-4487(96)00157-6.

Baker, P.A., Seltzer, G.O., Fritz, S.C., Dunbar, R.B., Grove, M.J., Tapia, P.M., Broda, J.P., 2001. The history of South American tropical precipitation for the past 25,000 years. Science 291, 640–643. https://doi.org/10.1126/science.291.5504.640.

Bøtter-Jensen, L., Andersen, C.E., Duller, G.A., Murray, A.S., 2003. Developments in radiation, stimulation and observation facilities in luminescence measurements. Radiat. Meas. 37, 535–541. https://doi.org/10.1016/S1350-4487(03)00020-9.

Capaldi, T.N., Rittenour, T.M., Nelson, M.S., 2022. Downstream changes in quartz OSL sensitivity in modern river sand reflects sediment source variability: Case studies from Rocky Mountain and Andean rivers. Quaternary Geochronology 71, 101317. https://doi.org/10.1016/j.quageo.2022.101317.

Cheng, H., Sinha, A., Cruz, F., Wang, X., Edwards, R.L., d'Horta, F.M., Auler, A.S., 2013. Climate change patterns in Amazonia and biodiversity. Nat. Commun. 4, 1411. https://doi.org/10.1038/ncomms2415.

del Río, I., Sawakuchi, A.O., Góes, A.M., Hollanda, M.H., Furukawa, N.Y., Porat, N., Negri, F.A., 2021. Luminescence signals of quartz and feldspar as new methods for stratigraphic discrimination and provenance analysis of siliciclastic successions: the case of the Parnaíba Basin (Brazil) of West Gondwana. Basin Res. 1–22. https://doi.org/10.1111/bre.12590.

Espurt, N., Baby, P., Brusset, S., Roddaz, M., Hermoza, W., Barbarand, J., 2009. The nazca ridge and uplift of the Fitzcarrald Arch: implications for regional geology in northern South America. In: Hoorn, C., Wesselingh, F.P. (Eds.), Amazonia: Landscape and Species Evolution: A Look into the Past. Wiley-Blackwell. https://doi.org/10.1002/9781444306408.ch6.

Filizola, N., Guyot, J.L., 2009. Suspended sediment yields in the Amazon basin: an assessment using the Brazilian national data set. Hydrol. Process. 23, 3207–3215. https://doi.org/10.1002/hyp.7394.

Gray, H.J., Jain, M., Sawakuchi, A.O., Mahan, S.A., Tucker, G.E., 2019. Luminescence as a sediment tracer and provenance tool. Rev. Geophys. 57, 987–1017. https://doi.org/10.1029/2019RG000646.

Haddadchi, A., Olley, J., Pietsch, T., 2016. Using LM-OSL of quartz to distinguish sediments derived from surface-soil and channel erosion. Hydrol. Process. 30, 637–647. https://doi.org/10.1002/hyp.10646.

Häggi, C., Chiessi, C.M., Merkel, U., Mulitza, S., Prange, M., Schulz, M., Schefuß, E., 2017. Response of the Amazon rainforest to late Pleistocene climate variability. Earth Planet Sci. Lett. 479, 50–59. https://doi.org/10.1016/j.epsl.2017.09.013.

Heimdal, T.H., Callegaro, S., Svensen, H.H., Jones, M.T., Pereira, E., Planke, S., 2019. Evidence for magma–evaporite interactions during the emplacement of the central atlantic magmatic province (CAMP) in Brazil. Earth Planet Sci. Lett. 506, 476–492. https://doi.org/10.1016/j.epsl.2018.11.018.

Hoppner, N., Lucassen, F., Chiessi, C.M., Sawakuchi, A.O., Kasemann, S.A., 2018. Holocene provenance shift of suspended particulate matter in the Amazon River basin. Quat. Sci. Rev. 190, 66–80. https://doi.org/10.1016/j.quascirev.2018.04.021.

Jaillard, E., Hérail, G., Monfret, T., Díaz-Martínez, E., Baby, P., Lavenu, A., Dumont, J.F., 2000. In: Cordani, U.G., Thomaz-Filho, A., Campos, D.A. (Eds.), Tectonic Evolution of the Andes of Ecuador, Peru, Bolivia and North-Ernmost Chile. Tectonic Evolution of South America. In: Acad. Bras. Cienc. Spec. Publ. 31st Int. Geol. Cong., pp. 41–95

Jain, M., Murray, A.S., Bøtter-Jensen, L., 2003. Characterisation of blue-light stimulated luminescence components in different quartz samples: implications for dose measurement. Radiat. Meas. 37, 441–449. https://doi.org/10.1016/S1350-4487(03)00052-0.

Jain, M., Choi, J.H., Thomas, P.J., 2008. The ultrafast OSL component in quartz: origins and implications. Radiat. Meas. 43, 709–714. https://doi.org/10.1016/j.radmeas.2008.01.005.

Kreutzer, S., 2020. In: Kreutzer, S., Burow, C., Dietze, M., Fuchs, M.C., Schmidt, C., Fischer, M., Friedrich, J. (Eds.), 2020. fit_CWCurve( ): Nonlinear Least Squares Fit for CW-OSL Curves -beta Version-. Function Version 0.5.2. Luminescence:

Comprehensive Luminescence Dating Data Analysis. R package version 0.9.7. https://CRAN.R-project.org/package=Luminescence.
Kreutzer, S., Schmidt, C., Fuchs, M.C., Dietze, M., Fischer, M., Fuchs, M., 2012. Introducing an R package for luminescence dating analysis. Ancient TL 30, 1–8.
Maia, R.G., Godoy, H.K., Yamaguti, H.S., Moura, P.A., Costa, F.S., Holanda, M.A., Costa, J.A., 1977. Projeto carvão no Alto Solimões: relatório final. Manaus: CPRM. Retrieved May 21, 2021, from. http://rigeo.cprm.gov.br/jspui/handle/doc/9392.
Mendes, V.R., Sawakuchi, A.O., Chiessi, C.M., Giannini, P.C., Rehfeld, K., Mulitza, S., 2019. Thermoluminescence and optically stimulated luminescence measured in marine sediments indicate precipitation changes over northeastern Brazil. Paleoceanogr. Paleoclimatol. 34, 1476–1486. https://doi.org/10.1029/2019PA003691.
Milani J., E., Zalán V., P., 1999. An outline of the geology and petroleum systems of the Paleozoic interior basins of South America. Episodes 22, 199–205. https://doi.org/10.18814/epiiugs/1999/v22i3/007.
Milliman, J.D., Syvitski, J.P., 1992. Geomorphic/tectonic control of sediment discharge to the ocean: the importance of small mountainous rivers. J. Geol. 100, 525–544.
Moquet, J.S., Guyot, J.L., Crave, A., Viers, J., Filizola, N., Martinez, J.-M., Pombosa, R., 2016. Amazon River dissolved load: temporal dynamics and annual budget from the Andes to the ocean. Environ. Sci. Pollut. Res. 23, 11405–11429. https://doi.org/10.1007/s11356-015-5503-6.
Moska, P., Murray, A.S., 2006. Stability of the quartz fast-component in insensitive samples. Radiat. Meas. 41, 878–885. https://doi.org/10.1016/j.radmeas.2006.06.005.
Murray, A.S., Wintle, A.G., 2000. Luminescence dating of quartz using an improved single-aliquot regenetative-dose protocol. Radiat. Meas. 32, 57–73. https://doi.org/10.1016/S1350-4487(99)00253-X.
Peng, J., Wang, X., Adamiec, G., Zhao, H., 2022. Critical role of the deep electron trap in explaining the inconsistency of sensitivity-corrected natural and regenerative growth curves of quartz OSL at high irradiation doses. Radiat. Meas. 159, 106874 https://doi.org/10.1016/j.radmeas.2022.106874.
Pietsch, T.J., Olley, J.M., Nanson, G.C., 2008. Fluvial transport as a natural luminescence sensitiser of quartz. Quat. Geochronol. 3, 365–376. https://doi.org/10.1016/j.quageo.2007.12.005.
Pupim, F.N., Sawakuchi, A.O., Almeida, R.P., Ribas, C.C., Kern, A.K., Hartmann, G.A., Cracraft, J., 2019. Chronology of Terra Firme formation in Amazonian lowlands reveals a dynamic Quaternary landscape. Quat. Sci. Rev. 210, 154–163. https://doi.org/10.1016/j.quascirev.2019.03.008.
Ribas, C.C., Aleixo, A., Nogueira, A.C., Miyaki, C.Y., Cracraft, J., 2012. A palaeobiogeographic model for biotic diversification within Amazonia over the past three million years. Proc. Biol. Sci. 279, 681–689. https://doi.org/10.1098/rspb.2011.1120.
Rossetti, D.F., Cohen, M.C., Tatumi, S.H., Sawakuchi, A.O., Cremon, É.H., Mittani, J.C., Moya, G., 2015. Mid-Late Pleistocene OSL chronology in western Amazonia and implications for the transcontinental Amazon pathway. Sediment. Geol. 330, 1–15. https://doi.org/10.1016/j.sedgeo.2015.10.001.
Ruokolainen, K., Moulatlet, G.M., Zuquim, G., Hoorn, C., Tuomisto, H., 2019. Geologically recent rearrangements in central Amazonian river network and their importance for the riverine barrier hypothesis. Frontiers of Biogreography 11. https://doi.org/10.21425/F5FBG45046.
Sawakuchi, A.O., Jain, M., Mineli, T.D., Nogueira, L., Bertassoli, D.J., Häggi, C., Cunha, D.F., 2018. Luminescence of quartz and feldspar fingerprints provenance and correlates with the source area denudation in the Amazon River basin. Earth Planet Sci. Lett. 492, 152–162. https://doi.org/10.1016/j.epsl.2018.04.006.
Sawakuchi, A.O., Rodrigues, F.C., Mineli, T.D., Mendes, V.R., Melo, D.B., Chiessi, C.M., Giannini, P.C., 2020. Optically stimulated luminescence sensitivity of quartz for provenance analysis. Methods and Protocols 3, 6. https://doi.org/10.3390/mps3010006.
Sawakuchi, A.O., Schultz, E.D., Pupim, F.N., Bertassoli, D.J., Souza, D.F., Cunha, D.F., Ribas, C.C., 2022. Rainfall and sea level drove the expansion of seasonally flooded habitats and associated bird populations across Amazonia. Nat. Commun. 13, 4945. https://doi.org/10.1038/s41467-022-32561-0.
Schneider, T., Bischoff, T., Haug, G.H., 2014. Migrations and dynamics of the intertropical convergence zone. Nature 513, 45–53.
Schobbenhaus, C., Bellizzia, A., 2001. Geological Map of South America, 1:5 000 000. CGMW - CPRM - DNPM - UNESCO, Brasília.
Sioli, H., 1984. The Amazon and its main affluents: hydrography, morphology of the river courses, and river types. In: Sioli, H. (Ed.), The Amazon. Springer, Dordrecht. https://doi.org/10.1007/978-94-009-6542-3_5.
Tassinari, C.C.G., Bittencourt, J.S., Geraldes, M.C., Macambira, M.J.B., Lafon, J.M., 2000. The Amazon craton. In: Cordani, U.G., Thomaz-Filho, A., Campos, D.A. (Eds.), Tectonic Evolution of South America. Acad. Bras. Cienc. Spec. Publ. 31st Int. Geol. Cong.
Thom, G., Xue, A.T., Sawakuchi, A.O., Ribas, C.C., Hickerson, M.J., Aleixo, A., Miyaki, C., 2020. Quaternary climate changes as speciation drives in the Amazon floodplains. Science Advances 6, eaax4718. https://doi.org/10.1126/sciadv.aax4718.
Tsukamoto, S., Nagashima, K., Murray, A.S., Tadad, R., 2011. Variations in OSL components from quartz from Japan sea sediments and the possibility of reconstructing provenance. Quat. Int. 234, 182–189. https://doi.org/10.1016/j.quaint.2010.09.003.
van Breukelen, M.R., Vonhof, H.B., Hellstrom, J.C., Wester, W.C., Kroon, D., 2008. Fossil dripwater in stalagmites reveals Holocene temperature and rainfall variation in Amazonia. Earth Planet Sci. Lett. 275, 54–60. https://doi.org/10.1016/j.epsl.2008.07.060.
Wang, X., Edwards, R., Auler, A., et al., 2017. Hydroclimate changes across the Amazon lowlands over the past 45,000 years. Nature 541, 204–207. https://doi.org/10.1038/nature20787.
Wintle, A.G., 2008. Luminescence dating: where it has been and where it is going. Boreas 37, 471–482. https://doi.org/10.1111/j.1502-3885.2008.00059.x.
Wintle, A.G., Adamiec, G., 2017. Optically stimulated luminescence signals from quartz: a review. Radiat. Meas. 98, 10–33. https://doi.org/10.1016/j.radmeas.2017.02.003.
Zhou, J., Lau, K.M., 1998. Does a Monsoon climate exist over South America? J. Clim. 11, 1020–1104.